New Insights into the Catalytic Cycle of Plant Nitrite Reductase. Electron Transfer Kinetics and Charge Storage[†]

Pierre Sétif,*[,‡] Masakazu Hirasawa,[§] Nicolas Cassan,[‡] Bernard Lagoutte,[‡] Jatindra N. Tripathy,[§] and David B. Knaff[§]

CEA, iBiTecS, F-91191 Gif sur Yvette, France, CNRS, URA 2096, F-91191 Gif sur Yvette, France, and Department of Chemistry and Biochemistry, Texas Tech University, Lubbock, Texas 79409-1061

Received November 13, 2008; Revised Manuscript Received January 27, 2009

ABSTRACT: Nitrite reductase, which reduces nitrite to ammonium in a six-electron reaction, was characterized through kinetic analysis of an electron transfer cascade involving photoexcited Photosystem I and ferredoxin. This cascade was studied at physiological pH by flash-absorption spectroscopy. Two different forms of the enzyme were studied: one isolated from spinach leaf and one histidine-tagged recombinant form. When the enzyme is oxidized in the absence of nitrite, single-enzyme reduction leads mostly to siroheme reduction with the leaf enzyme, whereas the siroheme and the [4Fe-4S] cluster are both reduced in equivalent amounts in the recombinant enzyme. When combined with the results of deazaflavin/EDTA photoreduction experiments, these data support a 50 mV negative shift of the siroheme midpoint potential in the recombinant enzyme. Despite this difference, the two forms of the enzyme exhibit similar values for the rate constant of single reduction by reduced ferredoxin (1200 s^{-1}) and for k_{cat} (420−450 electrons per second and per nitrite reductase). When nitrite reductase is initially pre-reduced to the state ferrous siroheme-NO•, the fast kinetics of reduction by ferredoxin and the thermodynamics of ferredoxin binding are equivalent to those observed with oxidized nitrite reductase without nitrite. Spectral and kinetic analyses of single reduction of the recombinant enzyme in the ferrous siroheme-NO• state by photoreduced ferredoxin reveal that this process leads to reduction of the [4Fe-4S] cluster with little, if any, NO• reduction. These data show that the enzyme must wait for the next reduction step before NO• undergoes substantial reduction.

In oxygenic phototrophs, nitrogen assimilation involves two sequential reactions that accomplish the reduction of nitrate to ammonia. In algae and higher plants that are incapable of independent nitrogen fixation, this is the only pathway for making nitrogen available at the redox level found in most nitrogen-containing biomolecules. Ferredoxin: nitrite oxidoreductase (EC 1.7.7.1), commonly called nitrite reductase (NiR),[1] catalyzes the second step in this process, the reduction of nitrite to ammonia, a reaction that involves six electrons and eight protons. Ferredoxin-dependent nitrite reductases have been isolated from a number of higher plants, algae, and cyanobacteria (*1*). They contain two prosthetic groups, a siroheme, and an iron−sulfur cluster. Siroheme is an Fe isobacteriochlorin that is uniquely present in nitrite and sulfite reductases. The three-dimensional structure of the recombinant form of the spinach enzyme, which contains an N-terminal His tag, has recently been determined to a resolution of 2.8 Å (*2*). Although most of the enzyme is well-defined in this structure, the N-terminal part comprising the His tag and the first 21 residues of the spinach enzyme were not visible. The cluster, which is of the [4Fe-4S] type, is coordinated to four cysteine residues with a sulfur atom of one cysteine also serving as an axial ligand to the siroheme group, as it was previously seen in the mechanistically related hemoprotein subunit of sulfite reductase from *Escherichia coli* (*3*). NiR has only one ferredoxin (Fd) binding site (*4*), and the structures of the spinach enzyme and of the major chloroplastic isoform of spinach Fd were used to build a model of the 1:1 complex with Fd (*2*). This model and data from chemical modification and site-directed mutagenesis studies suggest that Fd supplies the acidic residues and NiR the basic residues involved in complex formation and stabilization (*1, 5, 6*). From the relative cofactor distances deduced from this model building, it was suggested that, within the complex, electron transfer occurs preferentially from the [2Fe-2S] cluster of Fd to the NiR [4Fe-4S] cluster. As the midpoint redox potential (E_m) of the siroheme had

[†] This work was supported by the European Commission (NEST STREP SOLAR-H Contract 516510 and EU FP7-ENERGY-2007-1-RTD SOLAR-H2 to P.S.) and by the Chemical Sciences, Geosciences and Biosciences Division, Office of the Basic Energy Sciences, Office of Sciences, U.S. Department of Energy (Contract DE-FG03-99ER20346 to D.B.K.), for funding the production of all of the proteins used in this study and for portions of the experimental design and interpretation of the data.

* To whom correspondence should be addressed: CEA, iBiTecS, F-91191 Gif sur Yvette, France, or CNRS, URA 2096, F-91191 Gif sur Yvette, France. Phone: 33 1 69089867. Fax: 33 1 69088717. E-mail: pierre.setif@cea.fr.

[‡] CEA and CNRS.

[§] Texas Tech University.

[1] Abbreviations: DAF, deazaflavin; DCPIP, 2,6-dichlorophenolindophenol; E_m, midpoint redox potential; ET, electron transfer; F_A and F_B, two [4Fe-4S] clusters, the terminal electron acceptors of Photosystem I; Fd, ferredoxin; Fd_{ox} and Fd_{red}, oxidized and reduced ferredoxin, respectively; NiR, nitrite reductase; NiR_{ox} and NiR_{red}, oxidized and singly reduced nitrite reductase, respectively; NiR_{spl}, nitrite reductase purified from spinach leaves; NiR_{rec}, recombinant nitrite reductase overexpressed in *Escherichia coli*; P700, primary electron donor of Photosystem I; PSI, Photosystem I; WT, wild type.

10.1021/bi802096f CCC: $40.75
Published on Web 02/18/2009

been found to be more positive than that of the [4Fe-4S] cluster [−290 mV vs −365 mV (*7*)], reduction of the siroheme would involve the transient reduction of the NiR cluster.

The biochemical, electron paramagnetic resonance (EPR), resonance Raman, and absorption properties of NiR in different redox states and with different ligands bound to the siroheme have been studied by several groups (*7*−*13*). It was also shown that a complex of ferrous siroheme with $NO^{\bullet}$ (siroheme $Fe^{2+}-NO^{\bullet}$ state) can be formed during enzyme turnover and also by simple incubation of the oxidized enzyme with an excess of nitrite and ascorbate (*14*). This complex, which behaves as a true reaction intermediate, is reduced by two electrons compared to oxidized NiR. The rate of formation of the complex between nitrite and the oxidized enzyme is far too slow to be compatible with it serving as a kinetically competent intermediate, and in all likelihood, the enzyme is first reduced by one electron during turnover, a reaction which is followed by rapid binding of nitrite and a subsequent one-electron reduction to the siroheme $Fe^{2+}-NO^{\bullet}$ state. Hydroxylamine (NH_2OH) was proposed as a later intermediate. The complex of oxidized NiR with NH_2OH would be reduced by two more electrons than the complex of ferrous siroheme with $NO^{\bullet}$, in line with a proposed reaction scheme where catalysis advancement occurs by steps of two reducing equivalents (*14*). However, the evidence supporting the involvement of hydroxylamine as a reaction intermediate is weak, and much remains to be understood with regard to the late steps of the catalytic cycle.

In this work, we studied the electron transfer cascade from Photosystem I (PSI) to NiR by flash-absorption spectroscopy. This cascade is triggered by PSI photoexcitation leading to the reduction of Fd, which then acts as an intermediate electron carrier for NiR reduction. Kinetic measurements were performed under conditions of either single NiR reduction or multiple catalytic turnover. A detailed comparison was made between the enzyme isolated from spinach leaf and its recombinant form. Due to greater enzyme availability, the study of the recombinant enzyme was pursued much more extensively, in particular by comparing the kinetics and spectra for single reduction with NiR initially prepared in two different redox states, either oxidized without substrate or in the siroheme $Fe^{2+}-NO^{\bullet}$ state. New kinetic data were obtained using this approach, and the catalytic mechanism of nitrite reductase was further elucidated.

EXPERIMENTAL PROCEDURES

Biological Materials. All experiments were performed with PSI monomers isolated from the cyanobacterium *Synechocystis* sp. PCC 6803 and recombinant Fd from the same organism. PSI monomers, both from wild-type (WT) *Synechocystis* sp. PCC6803 (hereafter called *Synechocystis* 6803) and from a site-directed mutant of the PsaD extrinsic subunit [E105Q (*15*)], were purified using the procedure of Rögner et al. (*16*). This PsaD subunit is known to be involved, along with the two other extrinsic subunits, PsaC and PsaE, in binding Fd (see ref *17* for a review). Recombinant Fd encoded by the *fed1* gene from the cyanobacterium *Synechocystis* 6803 was expressed in *Escherichia coli* and purified according to the method described in ref *18*. The Fd concentration was estimated by assuming an absorption coefficient of 9.7 mM^{-1} cm^{-1} at 422 nm (*19*). Flash-absorption experiments were conducted at 295 K, in 20 mM Tricine (pH 8.0) and 4 mM potassium phosphate (pH 7.8), in the presence of 2 mM sodium ascorbate, 30 mM NaCl, 5 mM $MgCl_2$, and 0.03% *n*-dodecyl β-D-maltoside. The PSI concentration was calculated by assuming an absorption coefficient of 7740 M^{-1} cm^{-1} for $P700^+$ at 800 nm, as measured recently (*20*) [P700, a chlorophyll *a*−chlorophyll *a*′ heterodimer, is the primary electron donor of PSI (*21*)]. 2,6-Dichlorophenolindophenol (DCPIP) was used as a redox mediator for $P700^+$ reduction (25 μM for all experiments except 4 μM in Figure S5 of the Supporting Information).

Spinach nitrite reductase (EC 1.7.7.1) was prepared from spinach leaves using the procedure of Hirasawa et al. (*22*). The UV−visible absorption spectrum of the purified enzyme exhibits maxima at 278, 390 (Soret), and 573 nm, as previously reported (*8, 23*). Recombinant spinach nitrite reductase, which contains an N-terminal His tag, was expressed in *E. coli* and purified according to the method described in ref *2*. The enzyme exhibits absorbance maxima at 278, 392 (Soret), and 573 nm. Some of the measurements carried out in this study require an accurate value for the extinction coefficient of the enzyme, and because several different molar extinction coefficients were previously reported for chloroplastic NiR, i.e., 40 mM^{-1} cm^{-1} (*8, 9, 13, 14, 24*), 71 mM^{-1} cm^{-1} (*25*), and 79 mM^{-1} cm^{-1} (*12*) for the Soret absorption maximum, it was necessary to redetermine this value for the actual enzyme preparations used in this study. We measured this coefficient for the recombinant enzyme by the Pierce BCA assay, using a molecular mass of 68.3 kDa for the His-tagged apoenzyme (*26*), and found a value of 55 mM^{-1} cm^{-1} in two independent measurements. The iron content of NiR samples was determined by atomic absorption spectroscopy, using a Perkin-Elmer Zeeman 4110 ZL atomic absorption spectrometer. If one assumes the presence of five iron atoms per enzyme (one [4Fe-4S] cluster and one siroheme), the iron quantification corresponds to an absorption coefficient of 53 mM^{-1} cm^{-1}. This is close to the value determined using the BCA method and is consistent with EPR measurements in the $g = 4.3$ region showing that there is very little adventitious iron present in the oxidized enzyme (data not shown). We will use a value of 55 mM^{-1} cm^{-1} for the Soret absorption coefficient of the enzymes throughout the paper.

Flash-Absorption Measurements. The laser excitation (wavelength, 700 nm; duration, 6 ns; energy, 15 mJ) was provided by a dye laser (Continuum, Excel Technology) pumped by a Nd:YAG laser which was frequency doubled (Quantel). Laser excitation was saturating for PSI photochemistry. For measurements in the visible region, actinic effects of the measuring light (provided by a 200 W tungsten−halogen lamp) were kept minimal by opening a shutter only 1 ms before flash excitation and by decreasing the light intensity to a level where no actinic effect was observable. This level was adjusted according to the time scale and the wavelength of the measurement. The time response of the apparatus was adjusted between 1 and 100 μs with a varying charge resistor at the output of the measuring photodiode. At each wavelength, two interference filters of 10 nm FWHM were placed in the measuring beam before and after the sample cuvette. A biased silicium photodiode (type S3590-05 from Hamamatsu) was used as

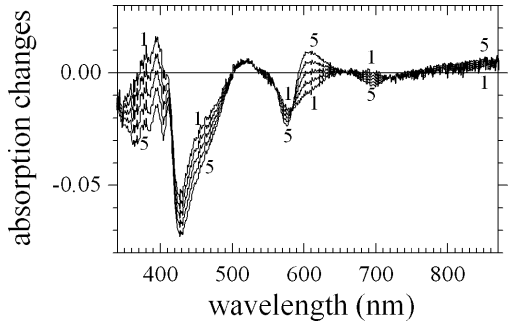

FIGURE 1: Calculated difference spectrum for reduction of the [4Fe-4S] cluster of NiR_{rec}. Spectra 1−5 were obtained by subtracting siroheme spectrum S_1 measured in NiR_{spl} (thick line spectrum of Figure S2B) from 3′ illumination difference spectrum S_2 of NiR_{rec} measured in the presence of deazaflavin and EDTA (dashed line spectrum of Figure S2A) with different multiplicative factors *f*: $S_2 - S_1 \times f$, where $f = 1.5$, 1.25, 1.0, 0.75, and 0.5 when going from spectrum 1 to spectrum 5. The middle spectrum is tentatively attributed to the [4Fe-4S] cluster reduction in NiR_{rec}.

the detector. The output signal was filtered and amplified using the 7A22 Tektronix (DC − ≤1 MHz) plug-in amplifier. The signals were recorded and digitized (Tektronix RTD710A) before being stored on a personal microcomputer for further treatment. Opening of the shutter led to some baseline distortion. This baseline was measured at each wavelength in the visible region with a cuvette containing water and was subtracted from the signals.

A wide range of PSI concentrations, from 0.20 to 20 μM, was used in different experiments. The cuvette width was adjusted, depending on the concentration, so that PSI photochemistry was saturated by laser excitation: 1 cm square cuvettes were used for PSI concentrations of <0.5 μM, 1 mm cuvettes for PSI in the 0.5−5 μM range, and 0.1 mm cuvettes (Hellman) for PSI above 5 μM. Cuvettes of 1 and 0.1 mm were placed at 45° angles to the measuring and exciting beams, leading to effective path lengths of 1.2 and 0.12 mm, respectively. As it is necessary that reduced Fd (Fd_{red}) or NiR be reoxidized between two consecutive flashes, it was important to avoid anaerobiosis. For this purpose, when using 1 and 0.1 mm cuvettes, the maximal number of flashes given to a sample was adjusted to keep the oxygen concentration of the solution above half of its normal value in air. This number of flashes was calculated assuming that O_2 was a two-electron terminal acceptor (assuming O_2 to be a four-electron acceptor would be less conservative). As a further control, it was shown that the absorption kinetics were unchanged during the whole period of study of a given sample. For signal averaging, the repetition rate of the flash experiments was 0.05−0.1 Hz. To ensure that the time interval between two flashes was sufficient for full relaxation of the absorption changes, the signals obtained under these conditions were shown to be identical to those obtained at a lower repetition rate (0.015−0.03 Hz).

Subtraction of Control Measurements. The data shown in Figures 2−5 involved subtraction of the flash-induced absorption changes measured in a control cuvette containing PSI and Fd, but no NiR. It was found that the $P700^+$ decay is similar in the control cuvette to that in the sample cuvette (containing NiR), so that the subtraction procedure allows the contribution of $P700^+$ to be eliminated. Moreover, after subtraction, the initial signals after the flash (up to ∼300 μs) were found to be close to the baseline (at any wavelength, <8% of the full signal after completion of NiR reduction). This shows that the kinetics of Fd photoreduction by PSI are little changed by NiR addition, so that they are also eliminated by the subtraction procedure, in line with the much higher affinity of Fd for PSI than for NiR (see Results). Moreover, for the measurements at 630 nm (Figure 2), the initial signals were indistinguishable from the baseline, as it could be expected from the very weak contribution of Fd reduction to the absorption changes [$\Delta(\Delta\varepsilon) < 100\ M^{-1}\ cm^{-1}$ for electron transfer from $(F_A,F_B)^-$ to Fd (unpublished data)].

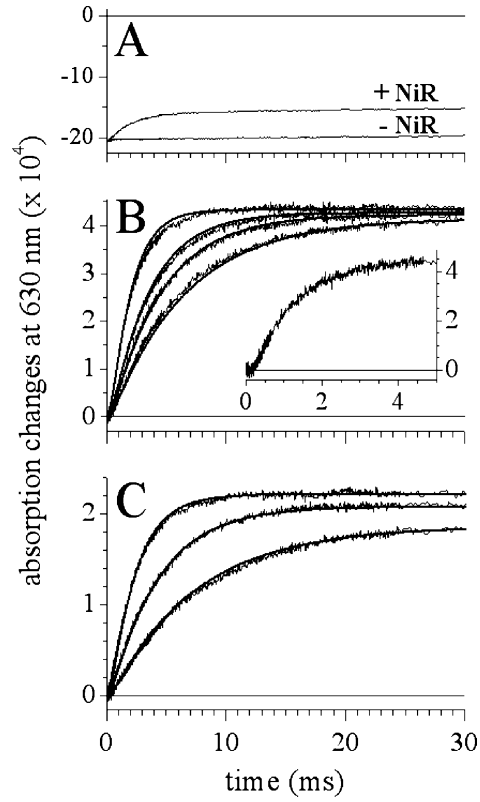

FIGURE 2: Flash-induced absorption changes measured at 630 nm with PSI, Fd, and NiR in the absence of nitrite. Absorption changes were measured for PSI/Fd and PSI/Fd/NiR mixtures on a 30 ms time scale. (A) Trace (−NiR), no NiR. Trace (+NiR), 2.33 μM NiR_{spl}. (B) Differences between absorption changes with and without NiR_{spl} at different NiR_{spl} concentrations of 0.58, 0.87, 1.16, and 2.33 μM when going from the slowest to the fastest kinetics. Smooth lines correspond to the best simulated fit according to the kinetic model described in the text. The best fit rate parameters are as follows: $k_{off} = 2100\ s^{-1}$, $k_1 = 2.6 \times 10^8\ M^{-1}\ s^{-1}$, and $k_{-1} = 3.0 \times 10^6\ M^{-1}\ s^{-1}$. In the inset, the difference (±NiR_{spl}) is shown for an experiment carried out with a NiR_{spl} concentration of 7.3 μM ([PSI] = 0.20 μM; [Fd] = 1.6 μM). (C) Conditions were similar to those described above but with the recombinant enzyme (NiR_{rec}) at 0.58, 1.15, and 2.34 μM. The best fit rate parameters are as follows: $k_{off} = 2400\ s^{-1}$, $k_1 = 1.9 \times 10^8\ M^{-1}\ s^{-1}$, and $k_{-1} = 1.0 \times 10^7\ M^{-1}\ s^{-1}$. Samples are contained in 1 cm optical path length cuvettes in the presence of 20 mM Tricine (pH 8.0), 5 mM $MgCl_2$, 30 mM NaCl, 4 mM potassium phosphate (pH 7.8), 2 mM sodium ascorbate, and 25 μM DCPIP. The PSI and Fd concentrations were 0.204 and 3.0 μM, respectively.

Fittings and Calculations. A global fit was used for fitting together either the four kinetic traces of Figure 2B or the three traces of Figure 2C. This fit was made with the Excel solver (version 2003, Microsoft) using eq 1 (see Results), with k_{off}, k_1, k_{-1} (the definitions of these rate constants are given below reactions 1 and 2 in Results) and a vertical scaling factor as free parameters.

The minimal value of the electron transfer rate k_{ET} within the Fd_{red}−oxidized NiR_{spl} complex was derived from the equation $k_{eff} = k_{ET}[k_{ET}/(k_{ET} + k_{dissoc})]$ and from the knowledge that k_{dissoc} equals 936 s^{-1} and the inequality $k_{eff} > 700$ s^{-1}. Combining the equation and the inequality gives $k_{ET}^2 - 700 \times k_{ET} - 6.55 \times 10^5 > 0$, the only positive root of the corresponding equality being a k_{ET} of 1200 s^{-1}. The inequality then gives $k_{ET} > 1200$ s^{-1}.

Spectrophotometric Measurements and Photoreduction with Deazaflavin. Difference spectra due to addition of nitrite or nitrite/ascorbate to NiR were measured in cuvettes with a path length of 1 cm with a 100 μL sample volume (model 105.202-QS from Hellma). For photoreduction experiments with deazaflavin, a similar cuvette was used. The sample containing recombinant NiR, 1 μM deazaflavin, and 2 mM EDTA was prepared in a glovebox (<20 ppm O_2), and the cuvette was closed with an airtight, turnover flange stopper. Deazaflavin was a kind gift from D. Florentin (Université Paris VI, Paris, France). Absorbance spectra were measured using a Uvikon-XL spectrophotometer.

RESULTS

In this paper, we performed electron transfer (ET) studies on two forms of NiR, either purified from spinach leaves (hereafter called NiR_{spl}) or overexpressed in *E. coli* (hereafter called NiR_{rec}). The recombinant form of the enzyme (NiR_{rec}) is His-tagged at its N-terminus. Though displaying similarities to NiR_{spl} in catalytic and spectral properties, some differences between the recombinant enzyme and the enzyme isolated from spinach leaves were previously observed (*26*). Part of this paper will be devoted to a comparison between the two enzyme forms. These studies have supplied access to new spectroscopic and kinetic information and, particularly from the NiR_{rec} data, provide some new insights into the catalytic mechanism of NiR.

Difference Spectra of NiR_{rec}. Similarities and Differences with NiR_{spl}. It is well documented that nitrite binds stoichiometrically to oxidized $[4Fe\text{-}4S]^{2+}/Fe^{3+}$ NiR, forming a 1:1 complex (*6, 8, 12, 24*). The difference spectrum due to nitrite binding to oxidized NiR_{rec} (see Figure S1 of the Supporting Information) is very similar to the spectrum which was determined previously with NiR_{spl} (*13*) and is virtually identical to the one previously recorded on another recombinant spinach NiR (*24*).

It has been reported that incubation of NiR_{spl} with nitrite and ascorbate induces the formation of the siroheme Fe^{2+}−$NO^{\bullet}$ complex (*14*), which had also been observed previously with vegetable marrow NiR (*27*). The corresponding $g \approx 2$ EPR signal is indicative of an $S = {}^1/_2$ spin which is best rationalized as involving a $NO^{\bullet}$ radical and a low-spin reduced iron (*13*). This experiment was repeated with NiR_{rec}, and both EPR and absorption signals were recorded. The EPR signal characteristic of the Fe^{2+} siroheme−$NO^{\bullet}$ complex was observed [$g_x = g_y = 2.06$ and $g_z = 2.007$ (*28*)]. The absorption changes were recorded by adding ascorbate to NiR_{rec} with nitrite already bound. From the optical difference spectra, which were recorded for different times of incubation with ascorbate (see Figure S1 of the Supporting Information), the lifetime of formation of the siroheme Fe^{2+}−$NO^{\bullet}$ complex was found to be 6 min, almost identical to that found with NiR_{spl} (*14*). The spectrum corresponding to the cumulative effects of nitrite and ascorbate addition (see Figure S1 of the Supporting Information) is very similar to the one found after prolonged incubation of NiR_{spl} with hydroxylamine (*8*). This confirms that incubation with hydroxylamine leads to the formation of the siroheme Fe^{2+}−$NO^{\bullet}$ complex, in agreement with previous EPR observations (*14*).

NiR_{rec} was also photoreduced by deazaflavin in the presence of EDTA (see Figure S2 of the Supporting Information), using a procedure which has been amply documented (see, e.g., refs *10* and *29*) and which has been previously used with NiR_{spl} using deazariboflavin (*7*). A striking observation of this experiment was that the [4Fe-4S] cluster was as easily photoreducible as the siroheme, as judged from the spectral shape of the difference spectrum induced by a short illumination time. Using this NiR_{rec} difference spectrum and a previously published redox difference spectrum of the siroheme in NiR_{spl}, we tentatively calculated the difference spectrum due to reduction of the [4Fe-4S] cluster in NiR_{rec}. This is shown in Figure 1, in which various amounts of the siroheme contribution were subtracted, leading to a family of five curves. It will be shown below that the middle spectrum is very close to what can be measured for the [4Fe-4S] cluster reduction of NiR_{rec} by flash-absorption spectroscopy.

Electron Transfer in a Ternary Mixture of PSI, Fd, and NiR in the Absence of Nitrite. In a ternary mixture of PSI, Fd, and NiR, an actinic flash is expected to trigger an ET cascade to NiR involving Fd as an intermediate. These different ET steps generate transient absorption changes that were monitored between 460 and 820 nm for NiR_{spl} (up to 950 nm for NiR_{rec}) by flash-absorption spectroscopy. Kinetics observed at 630 nm are displayed on a 30 ms time scale in the presence of Fd with or without NiR_{spl} (Figure 2A). The wavelength of 630 nm was chosen because of the relatively large contribution of NiR and because Fd reduction gives a negligible signal. Within PSI, charge separation between the primary donor P700 and the terminal acceptor (F_A,F_B) (two closely associated [4Fe-4S] clusters) is expected to occur within 1 μs (*17*). Under the conditions used here, a large part of PSI binds Fd, which results in fast Fd reduction, a process that is completed in a few hundred microseconds [not observable at 630 nm (*17*)]. It has been shown that the $P700^+$ decay is similar in the presence of Fd whether NiR is present or not. This allows the contribution of $P700^+$ to be eliminated by subtracting the (−NiR) kinetics from the (+NiR) kinetics (see Experimental Procedures). Such differences, obtained at different NiR_{spl} concentrations, are shown in Figure 2B on a 30 ms time scale. Similar differences measured with NiR_{rec} are shown in Figure 2C.

With both types of NiR, the resulting absorption changes have several distinct characteristics. They are sigmoidal, and the rate of signal rise increases, though not linearly, with NiR concentration. It can also be seen that, at low NiR concentrations, the final signal amplitude is smaller with NiR_{rec} than with NiR_{spl} and the kinetics of signal rise are slower (compare the two slower kinetics in panels B and C of Figure 2 measured with identical NiR concentrations). The smaller signal size indicates that the midpoint potential for the first reduction of NiR is more negative in NiR_{rec} than in NiR_{spl}. Using a model previously developed for a ternary mixture of PSI, Fd, and ferredoxin:$NADP^+$:oxidoreductase

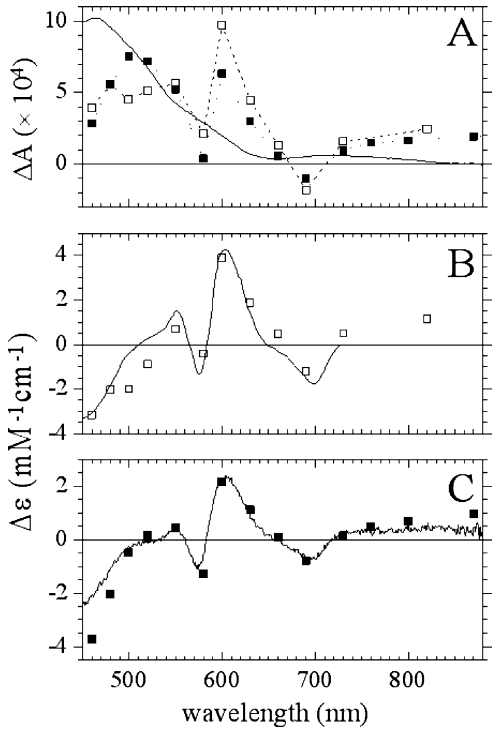

FIGURE 3: Difference absorption spectra from 460 to 870 nm of NiR reduction by Fd in the absence of nitrite under conditions favoring a single reduction. Signals measured at 950 nm (not shown) were identical to those measured at 870 nm. (A) Spectral data were obtained by flash absorption for NiR_{spl} (□) and NiR_{rec} (■) from kinetic traces similar to the traces shown in panels B and C of Figure 2, with 0.20 μM PSI (mutant E105Q of PsaD), 2.0 μM Fd, and 2.9 μM NiR_{spl} or NiR_{rec}. Signals were measured 14 and 20 ms after the flash for NiR_{spl} and NiR_{rec}, respectively. The absorption changes which are expected for the reoxidation of 0.20 μM Fd_{red} are shown as a solid line. (B) The contribution of NiR_{spl} reduction to the flash-absorption data is shown (□) after subtraction of the contribution of Fd reoxidation and is displayed in mM^{-1} cm^{-1} by assuming complete reduction of 0.20 μM oxidized NiR_{spl} by 0.20 μM Fd_{red}. The solid line was taken from a previous report (*7*) where it was attributed to siroheme reduction in NiR_{spl}. (C) The contribution of NiR_{rec} reduction to the flash-absorption data is calculated (■) as for panel B. The solid line spectrum is the spectrum shown in Figure S2B (thick line) due essentially, if not completely, to siroheme reduction in NiR_{rec}. In panels B and C, the vertical amplitudes of the continuous spectra were arbitrarily normalized to match approximately the flash-absorption signal at 600 nm.

(*20*), we will use the following simple kinetic scheme to model these kinetics:

$$(\text{PSI}-\text{Fd}) \xrightarrow{h\nu} (\text{PSI}-\text{Fd}_{red}) \xrightarrow{k_{off}} \text{PSI} + \text{Fd}_{red} \qquad \text{(I)}$$

$$\text{Fd}_{red} + \text{NiR}_{ox} \underset{k_{-1}}{\overset{k_1}{\rightleftharpoons}} \text{Fd}_{ox} + \text{NiR}_{red} \qquad \text{(II)}$$

PSI−Fd denotes the complex between PSI and Fd, and NiR_{red} and NiR_{ox} denote singly reduced and oxidized NiR, respectively. k_{off} is the dissociation rate constant of the ($PSI-Fd_{red}$) complex. k_1 and k_{-1} are the second-order rate constants for reduction of NiR_{ox} by Fd_{red} and for reduction of Fd_{ox} by NiR_{red}, respectively. Reaction I was introduced despite the fact that Fd reduction by PSI is not seen in these experiments. This is necessary because Fd_{red}, after being rapidly reduced, is not immediately available for NiR reduction as it must first dissociate from PSI. The simplifying assumptions of the above model were discussed in detail previously (*20*). One of its essential approximations is that NiR is reduced only once as it is present in excess over PSI (and therefore over Fd_{red} which is formed after PSI photoexcitation).

Such a model can be analytically solved under conditions where, at all times, NiR_{ox} is in excess over Fd_{red} and Fd_{ox} in excess over NiR_{red} (see ref (*20*).) according to the equation:

$$[\text{NiR}_{red}](t) = k_{red}[\text{PSI}-\text{Fd}_{red}]_{t=0}\left[\frac{-e^{-k_{off}t}}{k_{red}+k_{ox}-k_{off}} + \frac{k_{off}e^{-(k_{red}+k_{ox})t}}{(k_{red}+k_{ox}-k_{off})(k_{red}+k_{ox})} + \frac{1}{k_{red}+k_{ox}}\right] \qquad (1)$$

where $k_{red} = k_1[\text{NiR}]$ and $k_{ox} = k_{-1}[\text{Fd}]$. Using eq 1, we performed a global fit of all kinetics recorded at different NiR concentrations. The resulting simulated curves are superimposed with the experimental ones (Figure 2B,C). The best-fit parameters were as follows: with NiR_{spl}, $k_{off} = 2100$ s^{-1}, $k_1 = 2.6 \times 10^8$ M^{-1} s^{-1}, and $k_{-1} = 3.0 \times 10^6$ M^{-1} s^{-1}; with NiR_{rec}, $k_{off} = 2400$ s^{-1}, $k_1 = 1.9 \times 10^8$ M^{-1} s^{-1}, and $k_{-1} = 1.0 \times 10^7$ M^{-1} s^{-1}. The essential features of the experimental kinetics are in good agreement with the fits, with the relatively small deviations probably arising from oversimplifications in the model (e.g., 100% fast PSI−Fd intracomplex reduction of Fd, single NiR reduction, no explicit involvement of Fd−NiR complexes, no rate-limiting electron transfer step). The k_{off} values for dissociation of the ($PSI-Fd_{red}$) complexes are approximately equal to those previously measured with FNR as the electron acceptor of Fd_{red} (800 s^{-1} in ref *20* and 3200 s^{-1} in ref *30*). From the values of k_1 and k_{-1}, the redox equilibrium constant K_{eq} for reaction II can be calculated to be 87 and 19 for NiR_{spl} and NiR_{rec}, respectively. This constant is related to the difference in midpoint potentials of the reaction partners:

$$E_m(\text{NiR}_{ox}/\text{NiR}_{red}) - E_m(\text{Fd}_{ox}/\text{Fd}_{red}) = (RT/F) \times \ln(K_{eq}) \qquad (2)$$

Using the measured value of −412 mV for Fd from *Synechocystis* 6803 (*31*), one obtains −299 mV for the midpoint potential of the NiR_{ox}/NiR_{red} couple in the case of NiR_{spl}, which is close to the midpoint potential of −290 mV which was previously measured for the NiR siroheme by spectroelectrochemical titrations (*7*). The same calculation with NiR_{rec} gives a more negative midpoint potential of −338 mV. As already discussed in detail for the case of FNR (*20*), the k_1 values may not correspond to the true association rate constant k_{on} between Fd_{red} and NiR_{ox}, with k_1 being a lower limit for k_{on}. The rate constant k_{on} may thus be significantly larger than k_1, if one considers the likely possibility that dissociation of the $Fd_{red}-NiR_{ox}$ complex (k_{dissoc} rate) competes efficiently with electron transfer within the complex (k_{ET} rate).

The inset of Figure 2B displays kinetics obtained in a similar way but measured at a higher NiR_{spl} concentration (7.3 μM) and a somewhat different Fd concentration (1.6 μM). Half of the signal rise at 630 nm can be observed at 1.0 ms after flash excitation. This means that all steps leading to NiR reduction, including the effective ET rate (k_{eff}) between Fd_{red} and oxidized NiR, need to be faster that the corresponding rate of 700 s^{-1}. Moreover, in the simplest model that explicitly considers complex formation and

dissociation, k_{eff} is k_{ET} multiplied by the efficiency of electron transfer within the Fd_{red}−NiR complex, this efficiency being $k_{ET}/(k_{ET} + k_{dissoc})$. The rate k_{eff} is therefore a lower limit for the electron transfer rate constant k_{ET} from Fd_{red} to NiR_{ox} within the complex, due to competition between electron transfer and dissociation:

$$k_{eff} = k_{ET}[k_{ET}/(k_{ET} + k_{dissoc})] \quad (3)$$

This equation assumes that electron transfer within the complex is irreversible which, considering the large difference in midpoint potentials between ferredoxin and the enzyme, seems to be a valid approximation. The rate constant k_{dissoc} is not known but can be estimated from the knowledge of k_{on} (2.6×10^8 M^{-1} s^{-1}) and the dissociation constant K_d of the complex. Although this K_d is not known, some related parameters are known, such as the dissociation constant when both proteins are oxidized [$K_d \approx 6$ μM (see below)] and the Michaelis constant K_m (3.6 μM) for the Fd_{red} substrate (see below). To obtain a lower limit for k_{ET}, we take the lowest of these values (3.6 μM) for $K_d(Fd_{red}-NiR_{ox})$, which gives a k_{dissoc} ($=k_{on}K_d$) of 936 s^{-1}. From eq 3, with this value of k_{dissoc} and the inequality $k_{eff} > 700$ s^{-1}, one can deduce that k_{ET} is larger than 1200 s^{-1} (see Experimental Procedures). The signal observed here can be ascribed to reduction of the NiR_{spl} siroheme (see below). From the Fd_{red}−NiR state, reduction of the siroheme may consist of either a single step or two successive steps, if the [4Fe-4S] cluster of NiR_{spl} is reduced first. The calculations described above assume that only a single step is involved in NiR reduction but would be equally valid if siroheme reduction required two steps. In the latter case, our observations would impose two requirements. First, k_{ET} for reduction of the NiR iron−sulfur cluster would need to be larger than 1200 s^{-1}. Second, the rate of internal electron transfer from the cluster to the siroheme would need to be larger than 700 s^{-1}. A similar experiment was performed with NiR_{rec}, and a half-time of 1.2 ms ($k = 580$ s^{-1}) was observed with 1.6 μM Fd and 8 μM NiR_{rec}. Using the same approach described above [with values for $K_d(Fd_{red}-NiR_{ox})$ of 7 μM and k_{on} of 1.9×10^8 M^{-1} s^{-1}, resulting in a k_{dissoc} of 1300 s^{-1}], a value for k_{ET} of >1200 s^{-1} was also obtained.

Determination of the Fd−NiR Dissociation Constant in Two Redox States of NiR via Binding Competition Experiments. Reduction of ferredoxin by Photosystem I has been studied in detail by flash-absorption spectroscopy (*17, 32, 33*). Submicrosecond and microsecond phases of Fd reduction have been measured and assigned to first-order processes of Fd reduction within PSI−Fd complexes. The amplitude of these first-order phases can be used to probe the amount of complex present before flash excitation, and the dissociation constant K_d of the PSI−Fd complex can be determined from the dependence of these amplitudes upon ferredoxin concentration. In the presence of NiR, the apparent affinity of Fd for PSI thus measured is expected to decrease because of the competitive binding of Fd to NiR. Such an effect was observed for both NiR_{spl} (see Figure S3 of the Supporting Information) and NiR_{rec} in the oxidized state as well as in the siroheme $Fe^{2+}-NO^{\bullet}$ state and allowed us to derive the K_d values for the different NiR−Fd complexes (see the Supporting Information). Values of 5.7 ± 1.6 and 7.0 ± 2.1 μM were obtained for NiR_{spl} in the oxidized state and siroheme $Fe^{2+}-NO^{\bullet}$ state, respectively, whereas slightly larger values of 6.9 ± 2.5 and 7.3 ± 2.9 μM were found for the NiR_{rec}−Fd complexes. In view of the fitting uncertainties, it can be concluded that there are no significant differences between NiR_{spl} and NiR_{rec} with regard to their affinity for Fd. Moreover, with both types of NiR, the K_d values do not depend on the NiR redox state. K_d values for oxidized NiR had been measured previously by titration of spectral perturbations, with both NiR_{spl} and NiR_{rec} giving values in the 0.6−1.0 μM range (*5, 26*). The larger values determined here may result from the fact that different buffers, with different ionic strengths, were used (pH 8.0 instead of 7.5, and addition of 30 mM NaCl and 5 mM $MgCl_2$), as electrostatic interactions play an important role in formation of the complex between Fd and NiR (*2*). It should also be noted that the spectral perturbation measurements were carried out using ferredoxin from spinach, whereas the kinetic measurements used *Synechocystis* ferredoxin. Furthermore, the spectral perturbation measurements were made in the absence of any detergent, while small amounts of detergent used to solubilize the PSI reaction center are present in the kinetic measurement reaction mixtures.

Spectra for Reduction of Oxidized NiR by Photosystem I/Fd under Conditions Favoring Single-NiR Reduction. Kinetic measurements similar to those described in the legend of Figure 2 were used to determine the spectra between 460 and 950 nm corresponding to single reduction of NiR_{spl} and NiR_{rec} (2.9 μM in both cases). In both cases, NiR was oxidized before flash excitation and no nitrite was present. A PSI mutant (mutant E105Q of the PsaD subunit of PSI), which has a much higher affinity for Fd than WT PSI [$K_d = 0.015$ μM vs 0.4 μM for WT PSI (*15*)], was used for these measurements. With this mutant, NiR cannot compete efficiently with PSI for binding Fd and the reduction kinetics of Fd by PSI are identical regardless of whether NiR is present. Therefore, the kinetics without NiR could be exactly subtracted from those with NiR, providing a measurement of the kinetics of NiR reduction by Fd_{red} without any contributions from other reactions. Single reduction was favored by using a large excess of NiR over PSI (2.9 μM for both NiR vs 0.20 μM). Following the initial lag after the flash (which produces a sigmoidal shape at short times), a single rising component was observed at all wavelengths with half of the signal rise being observed at 1.4 ± 0.1 ms for NiR_{spl} (not shown) and 2.0 ± 0.2 ms for NiR_{rec} (Figure 4A,C). These kinetics are ~10% slower than those observed with WT PSI at similar NiR concentrations, suggesting that dissociation of the the PSI−Fd_{red} complex may be slightly slower in the PSI mutant. The NiR_{spl} and NiR_{rec} spectra shown in Figure 3A exhibit significant differences, with a smaller signal at 600 nm and a larger signal at 500−520 nm for NiR_{rec}. The spectra ascribed to NiR reduction were calculated after subtraction of the Fd contribution (Figure 3B,C) and were compared to the spectra ascribed to siroheme reduction, as measured by photoreduction by deaza(ribo)flavin/EDTA (thereafter called DAF spectra). For both NiRs, the shapes of the spectra measured by the two methods agree reasonably well, although significant differences can be seen. In the case of NiR_{spl} (Figure 3B), no obvious explanation is available for the differences seen with the two methods, with flash-induced signals being smaller than the DAF signals in the 500−550 nm region. In the case of NiR_{rec} (Figure 3C), the two spectra are in close agreement in the middle but, compared to the DAF spectrum, the flash-induced signals

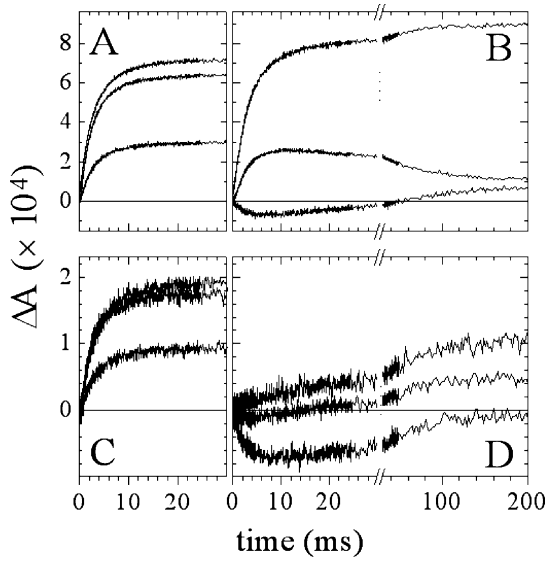

FIGURE 4: Kinetics of NiR_{rec} single reduction by Fd with NiR_{rec} prepared in two different redox states. The kinetics are shown at six different wavelengths, with 0.20 μM PSI (mutant E105Q of PsaD), 2.0 μM Fd, and 2.9 μM NiR_{rec}. (A and C) Kinetics observed on a 30 ms time scale with oxidized NiR_{rec}. (B and D) Kinetics observed with NiR_{rec} prepared in the siroheme $Fe^{2+}-NO^{\bullet}$ state on two different time scales (30 and 200 ms). (A and B) From top to bottom: 520, 600, and 630 nm. (C and D) From top to bottom: 870, 800, and 730 nm.

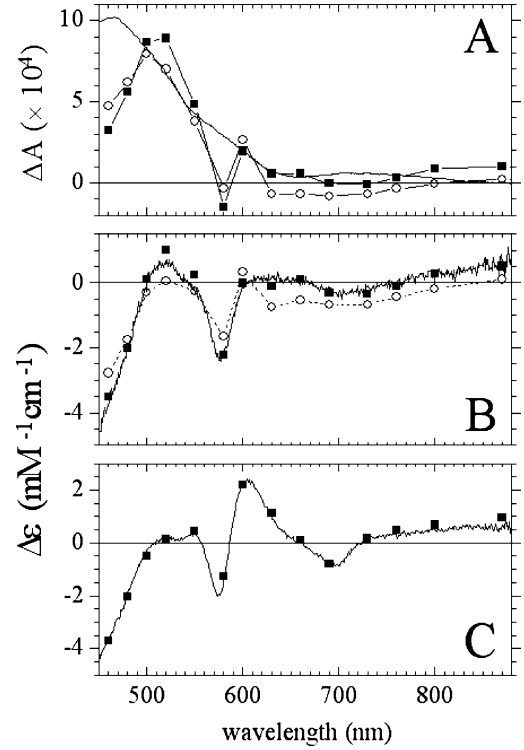

FIGURE 5: Difference spectra from 460 to 870 nm of NiR_{rec} reduction by Fd with NiR_{rec} prepared in two different redox states. Signals measured at 950 nm (not shown) were identical to those measured at 870 nm. (A) Spectra obtained from kinetic traces similar to traces shown in Figure 4 (B and D) with NiR_{rec} prepared in the siroheme $Fe^{2+}-NO^{\bullet}$ state, with 0.20 μM PSI (mutant E105Q of PsaD), 2.0 μM Fd, and 2.9 μM NiR_{rec}. Signals were measured 8 ms (○) and 200 ms after the flash (■). The absorption changes which are expected for the reoxidation of 0.20 μM reduced Fd are shown as a solid line. (B) The 8 and 200 ms spectra from panel A are plotted after subtraction of the ferredoxin contribution and displayed in units of mM^{-1} cm^{-1} by assuming a concentration of 0.20 μM. The solid line corresponds to the middle spectrum of Figure 1, after vertical adjustment for obtaining the best alignment with the 200 ms spectrum. (C) Spectrum obtained by flash-absorption spectroscopy for NiR_{rec} in the absence of nitrite (oxidized NiR_{rec} before flash excitation; same spectrum as shown in Figure 3C). This spectrum was fitted by a linear combination of the two spectra shown in Figure S4 for reduction of each NiR_{rec} cofactor, and the best fit is displayed as a solid line. It is obtained for equal amounts of reduction of the [4Fe-4S] cluster and the siroheme.

were smaller below 500 nm and larger above 800 nm. We were able to carry out more extensive studies with NiR_{rec}, because of the larger amounts of purified enzyme available. These studies, described below, have allowed us to show that [4Fe-4S] center reduction contributes significantly to the flash-absorption signals.

Single Reduction of NiR_{rec} by Photosystem I/Fd with NiR_{rec} Prepared in the Siroheme $Fe^{2+}-NO^{\bullet}$ State. As discussed above and as observed previously (*14*), NiR can be prepared in darkness in the siroheme $Fe^{2+}-NO^{\bullet}$ redox state by incubation with ascorbate and nitrite. The PSI/Fd/NiR_{rec} electron transfer cascade was studied under conditions where NiR_{rec} was prepared in this redox state and was in excess over PSI so that single reduction predominated. Under these conditions, we anticipate that the [4Fe-4S] cluster of NiR_{rec} will be first reduced by Fd_{red} and this may be followed by some substrate reduction. Flash-absorption kinetics (with or without NiR_{rec}) are shown in panels B and D of Figure 4, and the spectra derived from these kinetics are shown in Figure 5A. Kinetics of Figure 4 are shown at six different wavelengths (from top to bottom, 520, 600, 630, 870, 800, and 730 nm), and the kinetics obtained with oxidized NiR_{rec} under otherwise strictly identical conditions are shown for comparison in panels A and C of Figure 4. As already mentioned above, a single rising component was observed for oxidized NiR_{rec} with half of the signal rise being observed at 2.0 ± 0.2 ms. This is very different in the case of pre-reduced NiR_{rec} (siroheme $Fe^{2+}-NO^{\bullet}$ state), as two different components are observed. The kinetics of the fastest one are very similar to those found for oxidized NiR_{rec} with half of the signal rise being observed at 2.2 ± 0.2 ms, but with quite different amplitudes. Moreover, the slowest component, with a half-time of 45 ms, could be observed at all wavelengths.

The two spectra displayed in Figure 5A were measured 8 and 200 ms after the flash (○ and ■, respectively). After subtraction of the Fd contribution (solid line in Figure 5A), the spectra are displayed in Figure 5B in units of mM^{-1} cm^{-1} based on the concentration of photoreduced Fd (i.e., of PSI). In the same Figure 5B, the middle spectrum of Figure 1 is also plotted as a solid line, after vertical adjustment to produce the best alignment with the 200 ms spectrum. The family of spectra in Figure 1 were tentatively assigned as arising from the reduction of the NiR_{rec} [4Fe-4S] cluster. The almost perfect fit with the 200 ms spectrum gives a high level of confidence to the [4Fe-4S] difference spectrum derived from DAF measurements, and it shows that no significant $NO^{\bullet}$ reduction occurs under these conditions. The only reaction observed is cluster reduction. The fact that the 8 ms spectrum fits less satisfactorily with pure cluster reduction suggests that an intermediate state, different from the $[4Fe-4S]^{+}$ $Fe^{2+}-NO^{\bullet}$ state (with $[4Fe-4S]^{+}$ being the reduced state of the cluster), is populated at intermediate times. This point will be further discussed below. Double reduction of NiR_{rec} initially prepared in darkness in the [4Fe-

4S]$^{2+}$ $Fe^{2+}-NO^{\bullet}$ state was attempted by using a mixture of PSI, Fd, and NiR with a [PSI]/[NiR_{rec}] ratio close to 2 (data not shown). The kinetic and spectral complexity of the data is such that no clear interpretation can be given yet. This is due to incomplete Fd_{red} reoxidation and to different ET processes occurring together in the same time domain. Partial reoxidation of the siroheme was nevertheless observed under these conditions, which is consistent with the occurrence of $NO^{\bullet}$ reduction, but a quantitative assessment of these data requires much more investigation and is outside the scope of this study.

The flash-absorption spectrum recorded with oxidized NiR_{rec} [Figure 5C (■) and Figure 3C] was fitted with a linear combination of the two difference spectra measured with DAF and corresponding to reduction of each NiR cofactor (see Figure S4 of the Supporting Information). The resulting best-fit curve is shown as a solid line in Figure 5C and corresponds to 50% reduction of each cofactor. This suggests that the two redox cofactors of NiR_{rec} have similar midpoint potentials.

Midpoint Potentials and Redox Difference Spectra of the NiR_{rec} Cofactors. The difference spectra for reduction of each of the two NiR_{rec} cofactors are shown in Figure S4 of the Supporting Information. With these two spectra, it was possible to obtain almost perfect fits for the difference spectra in DAF photoreduction experiments (see the legend of Figure S4 for details). In turn, it was possible to estimate from these fits the difference in midpoint potentials between the two NiR_{rec} cofactors to be between −30 and −8 mV, with the [4Fe-4S] cluster having a higher E_m (see Figure S4 of the Supporting Information). Despite the large uncertainty in these estimations, these data suggest that the [4Fe-4S] cluster has a slightly more positive midpoint potential than the siroheme in NiR_{rec}, in contrast to the case of NiR_{spl}. Single reduction of oxidized NiR_{rec} in flash-absorption experiments points to similar potentials for both cofactors (see above). Taken together, both data sets suggest that the midpoint potential of the [4Fe-4S] cluster is equal or slightly more positive than that of the siroheme. Assuming equality, the value of −338 mV which was deduced from flash-absorption measurements corresponds to both midpoint potentials being −356 mV in NiR_{rec} {the 18 mV difference [$=(RT/F) \times \ln(2)$] results from an "entropic" contribution which corresponds to one cofactor or the other being reducible during single NiR reduction}. This value is very close to that measured for the NiR_{spl} [4Fe-4S] cluster [−365 mV (*7*); note, however, that, in this report, E_m was measured in the presence of the reduced siroheme], whereas it is considerably more negative than that of the NiR_{spl} siroheme [−290 mV (*7*), −299 mV from flash measurements in our study]. We can therefore conclude that the presence of the N-terminal extension containing the His tag in NiR_{rec} results in a significant decrease in the midpoint potential of the siroheme together with a much smaller effect on that of the [4Fe-4S] cluster.

An independent and more direct way of measuring the midpoint potentials of the NiR_{rec} cofactors would be highly desirable. Titrations of this sort are most commonly conducted using dithionite as a reductant, but the fact that dithionite and its oxidation products can act as ligands to siroheme at the nitrite-binding site makes this standard method inapplicable to siroheme-containing proteins (*34, 35*). Although spectroelectrochemical titrations have been used successfully to measure the midpoint redox potentials of the siroheme and [4Fe-4S] centers in NiR_{spl} (*7*), this technique was unsuccessful when applied to NiR_{rec} (*26*), giving poor fits to the $n = 1$ Nernst equation because of either poor redox equilibration with NiR_{rec} or nonspecific interactions between NiR_{rec} and the gold mini-grid electrode. Furthermore, it proved difficult to resolve the titration data into two phases with difference spectra arising from either only siroheme reduction or [4Fe-4S] cluster reduction (*26*). The data obtained in this study can provide at least a partial explanation for the earlier observations: When both cofactors have similar redox potentials, the reductive titration should initially result in parallel reduction of the two cofactors, and on further reduction, when doubly reduced NiR_{rec} accumulates, deviations from a standard Nernst curve should result from the electrostatic interaction between the two closely separated cofactors with similar midpoint potentials. The approach used in this study for measuring the midpoint potentials in NiR_{rec} provides an alternative method of measuring potentials in a case where usual methods are inapplicable.

Multiple Catalytic Turnover. When PSI and Fd are in large excess over NiR in the presence of nitrite, multiple turnovers of NiR can be monitored by following reoxidation of Fd_{red} which is initially reduced very rapidly by the terminal PSI acceptors. Such measurements are shown in Figure S5 of the Supporting Information. From these experiments, initial rates of Fd_{red} reoxidation can be obtained to calculate turnover rates, after subtraction of the rate of Fd_{red} reoxidation in the absence of NiR. With 5 μM PSI and a small excess of Fd (5.3 μM; Fd is almost entirely reduced after flash excitation), an initial rate of 260 reoxidized Fd_{red} molecules per second per NiR_{spl} was found. Reoxidation of Fd_{red} was also measured with Fd in large excess over PSI (5.0 μM PSI and 14 μM Fd). The kinetics of Fd_{red} reoxidation are then slower and correspond to a initial rate of 138 reoxidized Fd_{red} molecules per second per NiR_{spl}. This shows that Fd_{ox} is an inhibitor of Fd_{red} reoxidation, presumably because Fd binds to the same NiR site in both redox states. Experiments aimed at determining the type of inhibition (presumably competitive) and at measuring the inhibition constant could not be interpreted quantitatively in an unambiguous manner because of interference from Fd binding to PSI. Similar experiments performed with NiR_{rec} gave lower initial rates of Fd_{red} reoxidation. These rates were studied as a function of PSI concentration for both types of NiR (Figure S5 of the Supporting Information). These data were obtained by keeping the Fd concentration just above that of PSI [([Fd] − [PSI])/[PSI] ≤ 0.06] and were fitted by a Michaelis−Menten model (without inhibition): for NiR_{spl}, $K_m = 3.6 \pm 0.4$ μM and $k_{cat} = 425 \pm 20$ Fd_{red} molecules reoxidized per second per NiR_{spl}; for NiR_{rec}, $K_m = 14 \pm 2$ μM and $k_{cat} = 450 \pm 40$ Fd_{red} molecules reoxidized per second per NiR_{rec}). This shows that the smaller Fd_{red} reoxidation rates observed with NiR_{rec} are due to a higher K_m, whereas the k_{cat} values are almost identical for both types of NiR.

DISCUSSION

In this work, we performed a detailed study of ET kinetics by reconstituting in vitro the cascade of ET from PSI to NiR with photoreduced Fd as an intermediate ET carrier. ET was triggered by PSI photoexcitation, and the redox changes in

Table 1: Comparison of the Properties of the Spinach and Recombinant Forms of NiR

	NiR_{spl}	NiR_{rec}
single reduction of oxidized NiR by Fd_{red}		
redox equilibrium constant K_{eq} (reaction II)	87	19
midpoint potential $E_m(NiR_{ox}/NiR_{red})$[a] (mV)	−299	−338
$k_{off}(PSI-Fd_{red})$ (s^{-1})	2100	2400
second-order rate for single reduction of oxidized NiR[b] (M^{-1} s^{-1})	2.6×10^8	1.9×10^8
k_{ET} (intracomplex reduction of NiR by Fd_{red}) (s^{-1})	>1200	>1200
binding competition experiments		
$K_d(Fd_{ox}-NiR_{ox})$ (μM)	5.7 ± 1.6	6.9 ± 2.5
$K_d(Fd_{ox}-NiR_{red.NO})$[c] ($\mu$M)	7.0 ± 2.1	7.3 ± 2.9
catalysis measured by Fd_{red} reoxidation		
K_m (μM)	3.6 ± 0.4	14 ± 2
k_{cat} (Fd_{red} molecules s^{-1} NiR^{-1})	425 ± 20	450 ± 40

[a] Assuming $E_m = -412$ mV for the Fd_{ox}/Fd_{red} couple. [b] The given rate is a lower limit of the true second-order rate constant (see Results). [c] $NiR_{red.NO}$ stands for the siroheme $Fe^{2+}-NO^{\bullet}$ state.

NiR were recorded with NiR being initially (i.e., before flash excitation) prepared in two different redox states. Emphasis was placed on two main aspects. The first was a detailed comparison between NiR purified from spinach leaves (NiR_{spl}) and the recombinant form of spinach NiR, which carries an N-terminal His tag (NiR_{rec}). A detailed study of both enzyme forms provided new kinetic and thermodynamic information. The second was a detailed spectral characterization of the ET reactions occurring with NiR_{rec}, especially when prepared in the siroheme $Fe^{2+}-NO^{\bullet}$ state. This second approach has provided new knowledge about how NiR stores reducing equivalents on the cofactors and/or the substrate during catalysis.

Kinetic and Thermodynamic Properties of the Spinach Leaf and Recombinant NiR. Table 1 summarizes the comparison of kinetic, thermodynamic, and catalytic properties of the spinach and recombinant forms of NiR. Our flash-absorption experiments together with photoreduction experiments with DAF are consistent with a significant negative shift of the siroheme E_m in NiR_{rec} (approximately −50 mV), which results in both cofactors having similar E_m values. A few other characteristics of NiR_{rec} are different from those of NiR_{spl}: a slightly smaller second-order rate constant of reduction of oxidized NiR by Fd_{red} and a 4-fold higher Michaelis constant, $K_m(Fd_{red})$. Other parameters, such as the lower limit of the ET rate from Fd_{red} to oxidized NiR within the Fd−NiR complex, the dissociation constants (K_d) of the Fd−NiR complexes, and the catalytic rates (k_{cat}), are identical within experimental uncertainties. Similarities in K_d and k_{cat} parameters for the two NiR enzymes were previously reported, together with an increase in K_m in NiR_{rec} compared to that of NiR_{spl} (*26*). However, in this earlier report, K_m was found to increase 20-fold in NiR_{rec} (200 μM vs 10 μM), whereas we observe in this work an only 4-fold increase (14 μM vs 3.6 μM). The difference in experimental conditions (ionic strength, pH, and the presence or absence of detergent and $MgCl_2$) may be the reason for these discrepancies. It should also be noted that the spectral perturbation measurements reported in ref *26* were conducted out using ferredoxin from spinach, whereas the kinetic measurements presented here were conducted with *Synechocystis* ferredoxin. Another conclusion which can be drawn from the data presented here is that the His tag of NiR_{rec} does not significantly hinder ET from reduced Fd_{red} to NiR. This conclusion is consistent with the X-ray structure of the His-tagged enzyme, which shows that the His tag region is highly disordered (*2*). For both enzyme forms, the intracomplex reduction of NiR by Fd_{red}, which had not been measured before, was found to be faster than 1200 s^{-1}.

It was previously found that nitrite binding leads to a 17-fold increase in the K_d value for the Fd_{ox}−oxidized NiR_{spl} complex (*5*). In our light-driven experiments, probing oxidized NiR with bound nitrite was precluded due to the presence of ascorbate (required as part of the system used to reduce $P700^+$ between signal-averaging flashes) which leads to formation of the siroheme $Fe^{2+}-NO^{\bullet}$ state. However, we observed no significant difference in Fd binding between NiR prepared in the $Fe^{2+}-NO^{\bullet}$ state and oxidized NiR in the absence of nitrite (Table 1 and Figure S3 of the Supporting Information). This similarity is further substantiated by comparing the kinetics of NiR_{rec} reduction by Fd_{red} in the two redox states. Under the conditions described in the legend of Figure 4, oxidized NiR_{rec} is reduced by Fd_{red} with a half-time of 2.0 ms, a value quite similar to the half-time of 2.2 ms observed for the fast phase of NiR_{rec} reduction with NiR_{rec} in the siroheme $Fe^{2+}-NO^{\bullet}$ state. This fast phase represents the major step of electron transfer between Fd_{red} and partially reduced NiR_{rec}. We therefore conclude that Fd_{red} does not "sense" any difference between the two redox states of NiR_{rec}, and as shown in the binding competition measurements of Figure S3, Fd_{ox} also does not sense these. Moreover the fact that the [4Fe-4S] cluster is rapidly reduced when the siroheme is completely pre-reduced constitutes a direct proof that interprotein ET occurs from Fd to the [4Fe-4S] cluster which is then followed by intraprotein ET from the cluster to the siroheme (*2, 7*).

The Two NiR Cofactors Can Store Two Reducing Equivalents with Little or No Reduction of Bound NO$^{\bullet}$. Our flash-absorption data obtained with NiR_{rec} prepared in the $[4Fe-4S]^{2+}$ siroheme $Fe^{2+}-NO^{\bullet}$ redox state unambiguously show that reduction of the [4Fe-4S] cluster is followed by little $NO^{\bullet}$ reduction, up to 200 ms after the flash (Figures 4 and 5). If a significant reoxidation of the NiR_{rec} cofactors had occurred within this period, this would have led to major absorption changes, corresponding to siroheme and/or [4Fe-4S] cluster reoxidation. Such signals have not been observed, showing that almost no NiR_{rec} cofactor reoxidation is occurring within 200 ms of the flash. Therefore, the enzyme stores two negative equivalents on its two cofactors, presumably for use at later steps of the catalytic cycle. A more detailed analysis showed that, under such conditions, two exponential components are present with half-times of 2.2 and 45 ms. Moreover, after subtraction of the Fd contribution, the NiR_{rec} difference spectrum after completion of the two phases matches almost exactly the [4Fe-4S] redox difference spectrum that was calculated from DAF photoreduction measurements. This suggests that both cofactors are entirely reduced 200 ms after the flash ($[4Fe-4S]^+$ $Fe^{2+}-NO^{\bullet}$ state) with an intermediate state possibly involving a small extent of $NO^{\bullet}$ reduction (see Figure S6 of the Supporting Information for two alternative kinetic schemes proposing an interpretation of the biphasic kinetics). Despite some differences, NiR_{rec} and NiR_{spl} exhibit rather similar properties. The conclusion that a relatively stable state can be formed with both cofactors being reduced and $NO^{\bullet}$ bound to the siroheme is therefore most probably valid for NiR_{spl} as well. When NiR in this redox state binds Fd_{red}, this should necessarily

lead to extensive $NO^{\bullet}$ reduction as the enzyme cofactors cannot store any more reducing equivalents. This is supported by preliminary experiments which indicate that the siroheme is partially reoxidized under these conditions. However, studying $NO^{\bullet}$ reduction during catalysis, which is underway in the laboratory, requires much additional work before it can be quantitatively assessed.

ACKNOWLEDGMENT

B.L., N.C., and P.S. thank Ms. Véronique Mary for technical assistance. P.S. thanks Mr. Christian Chauvin and Mr. Louis Liagre for building cuvette holders, Dr. Dominique Florentin for his kind gift of deazaflavin, and Mrs. Thanh-Lan Lai for atomic absorption measurements.

SUPPORTING INFORMATION AVAILABLE

Figure S1 shows the difference absorption spectra of NiR_{rec} induced by nitrite binding and nitrite/ascorbate reduction. Figure S2 shows the difference absorption spectra of NiR_{rec} which was photoreduced in the presence of deazaflavin and EDTA. Figure S3 shows the competition between PSI and NiR_{spl} for Fd binding in two redox states of NiR_{spl}. Figure S4 shows the redox difference spectra of the [4Fe-4S] cluster and siroheme in NiR_{rec}. Figure S5 shows the kinetics of Fd_{red} reoxidation by NiR under conditions of multiple catalytic turnovers. Figure S6 shows two alternative kinetic schemes explaining the biphasic flash-absorption kinetics which are observed during single reduction of NiR_{rec} prepared in the siroheme $Fe^{2+}-NO^{\bullet}$ state. This material is available free of charge via the Internet at http://pubs.acs.org.

REFERENCES

1. Knaff, D. B. (1996) Ferredoxin and ferredoxin-dependent enzymes. In *Oxygenic Photosynthesis: The Light Reactions* (Ort, D. R., and Yocum, C., Eds.) pp 333−361, Kluwer Academic Publishers, Dordrecht, The Netherlands.
2. Swamy, U., Wang, M. T., Tripathy, J. N., Kim, S. K., Hirasawa, M., Knaff, D. B., and Allen, J. P. (2005) Structure of spinach nitrite reductase: Implications for multi-electron reactions by the iron-sulfur:siroheme cofactor. *Biochemistry 44*, 16054–16063.
3. Crane, B. R., Siegel, L. M., and Getzoff, E. D. (1995) Sulfite reductase structure at 1.6 Å: Evolution and catalysis for reduction of inorganic anions. *Science 270*, 59–67.
4. Knaff, D. B., and Hirasawa, M. (1991) Ferredoxin-dependent chloroplast enzymes. *Biochim. Biophys. Acta 1056*, 93–125.
5. Hirasawa, M., and Knaff, D. (1985) Interaction of ferredoxin-linked nitrite reductase with ferredoxin. *Biochim. Biophys. Acta 830*, 173–180.
6. Mikami, B., and Ida, S. (1989) Spinach ferredoxin-nitrite reductase: Characterization of catalytic activity and interaction of the enzyme with substrates. *J. Biochem. 105*, 47–50.
7. Hirasawa, M., Tollin, G., Salamon, Z., and Knaff, D. B. (1994) Transient kinetic and oxidation-reduction studies of spinach ferredoxin-nitrite oxidoreductase. *Biochim. Biophys. Acta 1185*, 336–345.
8. Vega, J. M., and Kamin, H. (1977) Spinach nitrite reductase. Purification and properties of a siroheme-containing iron-sulfur enzyme. *J. Biol. Chem. 252*, 896–909.
9. Lancaster, J. R., Vega, J. M., Kamin, H., Orme-Johnson, N. R., Orme-Johnson, W. H., Krueger, R. J., and Siegel, L. M. (1979) Identification of the iron-sulfur center of spinach ferredoxin-nitrite reductase as a tetranuclear center, and preliminary EPR studies of mechanism. *J. Biol. Chem. 254*, 1268–1272.
10. Krueger, R. J., and Siegel, L. M. (1982) Evidence for siroheme-Fe4S4 interaction in spinach ferredoxin-sulfite reductase. *Biochemistry 21*, 2905–2909.
11. Ondrias, M. R., Carson, S. D., Hirasawa, M., and Knaff, D. B. (1985) Characterization of the siroheme active site in spinach nitrite reductase by resonance Raman spectroscopy. *Biochim. Biophys. Acta 830*, 159–163.
12. Hirasawa, M., Shaw, R. W., Palmer, G., and Knaff, D. B. (1987) Prosthetic group content and ligand-binding properties of spinach nitrite reductase. *J. Biol. Chem. 262*, 12428–12433.
13. Kuznetsova, S., Knaff, D. B., Hirasawa, M., Sétif, P., and Mattioli, T. A. (2004) Reactions of spinach nitrite reductase with its substrate, nitrite, and a putative intermediate, hydroxylamine. *Biochemistry 43*, 10765–10774.
14. Kuznetsova, S., Knaff, D. B., Hirasawa, M., Lagoutte, B., and Sétif, P. (2004) Mechanism of spinach chloroplast ferredoxin-dependent nitrite reductase: Spectroscopic evidence for intermediate states. *Biochemistry 43*, 510–517.
15. Bottin, H., Hanley, J., and Lagoutte, B. (2001) Role of acidic amino acid residues of PsaD subunit on limiting the affinity of photosystem I for ferredoxin. *Biochem. Biophys. Res. Commun. 287*, 833–836.
16. Rögner, M., Nixon, P. J., and Diner, B. A. (1990) Purification and characterization of photosystem I and photosystem II core complexes from wild-type and phycocyanin-deficient strains of the cyanobacterium *Synechocystis* PCC 6803. *J. Biol. Chem. 265*, 6189–6196.
17. Sétif, P. (2001) Ferredoxin and flavodoxin reduction by photosystem I. *Biochim. Biophys. Acta 1507*, 161–179.
18. Barth, P., Guillouard, I., Sétif, P., and Lagoutte, B. (2000) Essential role of a single arginine of photosystem I in stabilizing the electron transfer complex with ferredoxin. *J. Biol. Chem. 275*, 7030–7036.
19. Tagawa, K., and Arnon, D. I. (1968) Oxidation-reduction potentials and stoichiometry of electron transfer in ferredoxins. *Biochim. Biophys. Acta 153*, 602–613.
20. Cassan, N., Lagoutte, B., and Sétif, P. (2005) Ferredoxin-$NADP^+$ reductase: Kinetics of electron transfer, transient intermediates, and catalytic activities studied by flash-absorption spectroscopy with isolated photosystem I and ferredoxin. *J. Biol. Chem. 280*, 25960–25972.
21. Jordan, P., Fromme, P., Witt, H. T., Klukas, O., Saenger, W., and Krauss, N. (2001) Three-dimensional structure of cyanobacterial photosystem I at 2.5 Å resolution. *Nature 411*, 909–917.
22. Hirasawa, M., Fukushima, K., Tamura, G., and Knaff, D. B. (1984) Immunochemical characterization of nitrite reductases from spinach leaves, spinach roots and other higher plants. *Biochim. Biophys. Acta 791*, 145–154.
23. Ida, S., and Mikami, B. (1986) Spinach ferredoxin-nitrite reductase: A purification procedure and characterization of chemical properties. *Biochim. Biophys. Acta 871*, 167–176.
24. Bellissimo, D. B., and Privalle, L. S. (1995) Expression of spinach nitrite reductase in *Escherichia coli*: Site-directed mutagenesis of predicted active-site amino-acids. *Arch. Biochem. Biophys. 323*, 155–163.
25. Vigara, J., Garcia-Sanchez, M. I., Garbayo, I., Vilchez, C., and Vega, J. M. (2002) Purification and characterization of ferredoxin-nitrite reductase from the eukaryotic microalga *Monoraphidium braunii*. *Plant Physiol. Biochem. 40*, 401–405.
26. Tripathy, J. N., Hirasawa, M., Kim, S. K., Setterdahl, A. T., Allen, J. P., and Knaff, D. B. (2007) The role of tryptophan in the ferredoxin-dependent nitrite reductase of spinach. *Photosynth. Res. 94*, 1–12.
27. Fry, I. V., Cammack, R., Hucklesby, D. P., and Hewitt, E. J. (1980) Stability of the nitrosyl-sirohaem complex of plant nitrite reductase, investigated by EPR spectroscopy. *FEBS Lett. 111*, 377–380.
28. Cammack, R., and Fry, I. V. (1980) Third-harmonic detection of electron-paramagnetic-resonance spectra: Resolution of the hyperfine splitting in nitrosylated nitrite reductase from vegetable marrow (*Cucurbita pepo*). *Biochem. Soc. Trans. 8*, 642.
29. Massey, V., and Hemmerich, P. (1978) Photoreduction of flavoproteins and other biological compounds catalyzed by deazaflavins. *Biochemistry 17*, 9–16.
30. Fourmond, V., Lagoutte, B., Sétif, P., Leibl, W., and Demaille, C. (2007) Electrochemical study of a reconstituted photosynthetic electron-transfer chain. *J. Am. Chem. Soc. 129*, 9201–9209.
31. Bottin, H., and Lagoutte, B. (1992) Ferredoxin and flavodoxin from the cyanobacterium *Synechocystis* sp. PCC 6803. *Biochim. Biophys. Acta 1101*, 48–56.
32. Sétif, P., and Bottin, H. (1994) Laser flash absorption spectroscopy study of ferredoxin reduction by photosystem I in *Synechocystis* sp. PCC 6803: Evidence for submicrosecond and microsecond kinetics. *Biochemistry 33*, 8495–8504.

33. Sétif, P., and Bottin, H. (1995) Laser flash absorption spectroscopy study of ferredoxin reduction by photosystem I: Spectral and kinetic evidence for the existence of several photosystem I-ferredoxin complexes. *Biochemistry 34*, 9059–9070.
34. Stoller, M. L., and Malkin, R. (1977) Oxidation-Reduction Properties of Photosynthetic Nitrite Reductase. *FEBS Lett. 81*, 271–274.
35. Day, E. P., Peterson, J., Bonvoisin, J. J., Young, L. J., Wilkerson, J. O., and Siegel, L. M. (1988) Magnetization of the sulfite and nitrite complexes of oxidized sulfite and nitrite reductases: EPR silent spin S = 1/2 states. *Biochemistry 27*, 2126–2132.

BI802096F